Inorganic Semiconductors for Printed Transistors

Brent Ridley
S.B. Chemistry 1996
Massachusetts Institute of Technology

Submitted to the Program in Media Arts and Sciences
School of Architecture and Planning

in partial fulfillment of the requirements for the degree of
Master of Science in Media Arts and Sciences
at the Massachusetts Institute of Technology
June 1999

Written by **Brent Ridley**
Program in Media Arts and Sciences
May 7 1999

Certified by **Joseph Jacobson**
Assistant Professor
Program in Media Arts and Sciences
Department of Mechanical Engineering
Thesis Advisor

Accepted by **Stephen Benton**
Chair of Departmental Committee on Graduate Students
Program in Media Arts and Sciences

Inorganic Semiconductors for Printed Transistors

Brent Ridley

Submitted to the Program in Media Arts and Sciences
School of Architecture and Planning
on May 7 1999

in partial fulfillment of the requirements for the degree of
Master of Science in Media Arts and Sciences

Massachusetts Institute of Technology

Abstract

CdSe nanoparticles have been solution deposited and thermally processed into thin film transistor channels, demonstrating for the first time that an inorganic semiconductor can be printed. A peak field effect mobility of 2.05 $cm^2V^{-1}s^{-1}$ was observed for a device processed at 350 °C. The highest ON/OFF ratio, found in a different device, was 8.6×10^3 for a 10 to -10 V gate sweep at a drain-source voltage of -5 V. For the same voltage sweep a mobility of 0.26 $cm^2V^{-1}s^{-1}$ and an ON/OFF ratio of 1.3×10^3 was observed in a single device. Processing temperatures as low as 250 °C were found to produce semiconducting films that displayed a field effect. A new metathetic synthesis was developed to produce pyridine-capped CdSe nanoparticles at sizes below 20 Å.

Joseph Jacobson
Thesis Advisor
Assistant Professor
Program in Media Arts and Sciences
Department of Mechanical Engineering

Inorganic Semiconductors for Printed Transistors

Brent Ridley

Submitted to the Program in Media Arts and Sciences
School of Architecture and Planning

in partial fulfillment of the requirements for the degree of
Master of Science in Media Arts and Sciences

Massachusetts Institute of Technology
June 1999

Thesis Committee

Joseph Jacobson
Assistant Professor
Program in Media Arts and Sciences
Department of Mechanical Engineering
Thesis Advisor

Dimitri Antoniadis
Ray and Maria Stata Professor of Electrical Engineering
MIT Department of Electrical Engineering and
Computer Science
Thesis Reader

Moungi Bawendi
W. M. Keck Professor of Energy
MIT Department of Chemistry
Thesis Reader

Inorganic Semiconductors for Printed Transistors

Brent Ridley
June 1999

Introduction

Synthesis

Deposition and Ordering

Inorganic Semiconductors for Printed Transistors

Brent Ridley
June 1999

Introduction

Limitations of Current Fabrication Technology

Current fabrication costs and methods prohibit electronic devices from finding applications where three-dimensional architectures, flexibility, disposability, and extremely large or small unit counts are required. The typical setup cost of a fabrication plant is greater than a billion dollars and electricity alone costs a million dollars a month. Fabrication is expensive, too, as depositing and annealing layers often requires high temperatures and a controlled atmosphere, and patterning and etching these layers generates a large amount of toxic waste.[1]

The high temperatures used in silicon (Si) processing prevent three-dimensional fabrication,[2] large area fabrication,[3] and are incompatible with heat sensitive materials such as organic and biological molecules. High temperatures also prohibit deposition onto low-cost flexible plastics. Today's rigid devices hinder the introduction of electronics into clothing and non-intrusive personal accessories, where a number of medical, information, and communication applications can be envisioned.[4]

Printing as a Route to Microelectronics Fabrication

A seemingly simple technology like printing addresses some of the shortcomings of traditional microelectronics fabrication. A key feature of printing is that it economically deposits materials only where they are needed. Spin-coating, often used in microelectronics fabrication to deposit photoresist, consumes ~100 times more material than a printing process such as ink jetting.[5] Many traditional processing steps require a flat substrate, while printing can deposit onto surfaces with arbitrary features.[6] Although temperature and resolution remain as hurdles, printing provides a model for the inexpensive and efficient fabrication of both flexible and rigid microelectronic devices.

While additive technologies like printing are attractive because of their efficiency and potentially low cost, they are not without fault. The insulators, semiconductors, and conductors used in device fabrication can have melting points well above 1000 °C,[7] preventing their liquid processing. As powders these materials can be printed and then sintered, but this still requires the high temperature processing used in current fabrication schemes.[8] The powder also limits the minimum film thickness and the lateral resolution of a printed feature, making it impossible to compete with modern circuitry.[9]

The resolution limits set by powdered materials are insignificant when compared to the resolution limits imposed by traditional printing. The best printing resolutions are on the order of 5000 dpi (dots per inch),[10] meaning that features as small as 1/5000th of an inch, or 5 μm, can be printed. State-of-the-art electronic devices have feature sizes as small as 0.25 μm, moving to 0.18 μm and 0.10 μm by 2005.[10] While 5 μm resolution allows the fabrication of respectable devices, the ultimate packing density, power consumption, and speed of such devices are limited by the relatively large features. In order for the economy and flexibility offered by printing to compete with current device fabrication, low temperature and high quality printable materials must be developed and the printing process itself must be advanced to allow the deposition of sub-micron features.

A recently developed printing technique known as microcontact printing (μCP) promises to address patterning at the sub-micron level. Pioneered by George Whitesides, μCP employs a micrometer or nanometer-scale patterned stamp to transfer a material to a substrate. Generally, a self-assembling monolayer is transferred and acts as an etch resist, and as such the process is not an entirely additive technique. Still, μCP and similar "soft lithography" methods[6] provide a route to all-printed devices.[11] Demonstrated resolutions can compete with modern devices and even the next generations of devices, as the deposition of features as small as 35 nm has been reported.[6]

Printable Organic Materials

A viable printing technology relies on printable device-quality materials. To date, the most promising materials have been organic conductors and semiconductors, and recently these materials have been the focus of a number of research efforts.[12]

Such materials do not require high temperature processing and are intrinsically printable if they are designed properly. However both the semiconducting and conducting properties of organics lag behind the performance of inorganic conductors and semiconductors (**TABLE 1**).

Semiconductors	**Mobility (μ) ($cm^2V^{-1}s^{-1}$)**	**Comments**
Organic		
P3HT (*p*-type)[13]	0.1	Spin-coated
Pentacene (*p*-type)[14]	1.8	
Inorganic[7]		
Si (*n*-type)	1900	
Si (*p*-type)	500	
GaAs (*n*-type)	8800	
GaAs (*p*-type)	400	
CdSe (*n*-type)	900	
Conductors	**Conductivity (σ) ($\Omega^{-1}cm^{-1}$)**	**Comments**
Organic		
Polyaniline[15]	300	Printed
Polyacetylene[16]	10^5	
Inorganic[7]		
Cr	8.0×10^4	
Al	3.8×10^5	
Au	4.5×10^5	
Cu	6.0×10^5	
Ag	6.3×10^5	

TABLE 1: Comparison of organic and inorganic semiconductors and conductors

Organic semiconductor charge carrier mobilities as high as 1.8 $cm^2V^{-1}s^{-1}$ have been reported in vacuum-deposited pentacene,[14] and although this mobility is comparable to that of the amorphous silicon (α-Si) used in active matrix fabrication,[17] it is near pentacene's upper limit and is not suitable for logic. The row and column drivers for an active matrix liquid crystal display (AMLCD) require mobilities of 40,[18] clearly beyond pentacene's capabilities. Furthermore pentacene is not printable and the best-printed organic semiconductor, poly(3-

hexylthiophene) (P3HT), has demonstrated a lower mobility of 0.1 $cm^2V^{-1}s^{-1}$.[13] Both experiment and theory suggest that organic semiconductors have peak mobilities of ~1 $cm^2V^{-1}s^{-1}$ or less,[19,20] forcing researchers to adopt non-traditional device structures to pass enough current through organic devices to drive display pixels.[20]

Despite the utility of organic materials in low-end applications such as smart cards,[21] tags,[10] and active matrices,[12] they are not suitable for logic and a number of logic intensive applications exist for flexible electronics. In addition to wearable and ubiquitous computing,[4] electronic books[22] depend upon printed electronics. Printed electronics are especially well-suited for this application as the display medium itself can be printable.[23] For a truly paper-like display, pixel resolution will be higher than current displays, requiring pixel transistors with mobilities better than α-Si.[18] Also, the many displays in a book or newspaper require row and column drivers similar to those in AMLCDs. Such drivers cannot be made with organic materials and even if a traditional fabrication could provide a flexible solution, the cost of 100 pages worth of complex driver circuitry would be cost prohibitive.

Printable Inorganic Materials

Due to the limited applications of organic semiconductors and the outstanding need for printable high-mobility semiconductors, it is desirable to overcome the resolution and high temperature hurdles associated with the printing of inorganic powders. When coupled with advances in μCP, inorganic materials can be printed at high resolutions and low temperatures by using a nanoparticle-based ink. Unlike finely ground inorganic particles, which at their smallest are 300 nm[10] and are large enough to retain the properties of the bulk material, nanocrystalline materials display properties somewhere between those of an atom and a bulk crystal.[24] At particle sizes below 5 nm there is a large melting point depression that allows low temperature processing of the nanoparticles into polycrystalline films.[25,26] The reliable feature sizes of such films are only limited to sizes 5 to 7 times the diameter of the deposited nanoparticles,[9] and nanoparticles readily suspend in appropriate solvents,[27] making them ideal candidates for printing.

Nanoparticles, also known as quantum dots or artificial atoms, require ligand stabilizers to prevent particle agglomeration.[28] Such "capping groups" are generally introduced to the particles during their formation, but can be exchanged after synthesis is complete.[24,27] Because of their extremely small size, nanoparticles cannot be formed by grinding, but are instead synthesized by a number of chemical means, including solution-phase chemistry,[29] physical vapor deposition,[30] and etching.[31]

Ideally, the conversion of nanoparticles into bulk films proceeds through two stages. First, the capping group leaves the surface, leaving a purely nanocrystalline array of particles in contact with each other. Then, upon further heating, the particles melt, nucleate, and grow crystals.

Though conceived independently, the notion of using nanoparticles as precursors for thin films has been proposed by other researchers.[25,32] Despite a handful of references in papers[25,32] and a few patents, [33,34,35] there have been only two related studies in which semiconductor nanoparticles were used as precursors for a polycrystalline film in a device.[36,37,38] In the more successful of those studies, a methanol-based cadmium telluride (CdTe) colloid was spray-deposited onto a hot substrate as a part of solar cell fabrication.[37] Device performances were never discussed in the numerous publications from this project,[37,38,39,40,41] but related publications mention that a 2,793 cm^2 device has displayed an active area efficiency of 10.5%.[38] While the success of this approach is heartening, spray deposition does not address the differences between the unpatterned thick films of solar cells and the finely patterned thin films required for microelectronics fabrication.

Cadmium Selenide Nanoparticles for Transistors

As with the work on organic electronics, this work focuses on the semiconductor. We have chosen to first work with the II-VI semiconductor CdSe because "the best developed semiconductor 'nanocrystal' synthesis is that of CdSe."[29] Since the 1960s CdSe has been deposited by standard vacuum techniques for thin film transistors (TFTs) and driver circuitry for active matrices.[42] Furthermore the unwanted formation of the oxide associated with CdSe does not pose as severe a problem as it does with Si (**TABLE 2**).

	Si	Cd	Se
Bond Strength With Oxygen ($kJmol^{-1}$)	800	236	465

TABLE 2: Comparison of the strength of oxygen binding to semiconductors.[7]

Using CdSe nanoparticles we have demonstrated the first printed inorganic semiconductor TFT channels. A field effect mobility as high as 2.05 $cm^2V^{-1}s^{-1}$ is observed and is to our knowledge the highest mobility ever observed in a printed semiconductor. For another device, at a drain-source voltage of -5 V, ON/OFF ratios as high as 8.6×10^3 are found for a gate sweep of 10 to -10 V. In a single device the best performance is an ON/OFF ratio of 1.3×10^3 and a mobility of 0.26 $cm^2V^{-1}s^{-1}$. Field effect activity is observed in films sintered as low as 250 °C, demonstrating that nanoparticle-based solution deposition can be a plastic-compatible process (≤ 400 °C).

Two published nanoparticle syntheses were examined, and after neither yielded particles appropriate for device fabrication, a modified metathesis approach was developed. This new synthesis forms CdSe particles of discrete sizes with loosely bound capping groups. In addition to the semiconducting and electrical characteristics of sintered nanoparticle films, particle size and stoichiometry and fused-film morphology and composition were studied.

Synthesis

Approaches to Nanoparticle Synthesis

A number of synthetic approaches have been used to synthesize nanoparticle conductors, semiconductors, and insulators.[43] Previous research on II-VI semiconductors synthesized nanoparticles by pyrolysis of organometallic precursors;[24,44,45] by arrested precipitation;[46] by precipitation in reverse micelles;[47] and by exchange, or metathesis, reactions.[48]

In selecting a nanoparticle synthesis, the purity, stoichiometry, size distribution, and yield are all issues to consider. The purity of the particles is fundamentally the most important because it directly effects the quality of the resultant semiconducting film. Reproducible stoichiometry is also critical to device performance, as an excess of one component in the semiconductor can act as a dopant.[49] In order to ensure low temperature processing, control over the particle size and distribution is important. Synthetic yield is crucial in a production setting but is not crucial in a research environment.

We have employed two synthetic routines to produce nanoparticles below 5 nm in diameter. Due to device process temperature considerations, particles 25 Å in diameter and smaller are of primary interest. The more complex pyrolysis scheme lacks high yields and a simple synthetic practice, but allows tight control of particle size and distribution.[24,27] Without modification the simpler metathesis approach does not provide tight control over particle size, shape, or distribution, but offers high yields, 1:1 stoichiometry, and tamer reaction conditions.[37,48] As published, neither procedure was found to be appropriate for this work, and so a modified metathesis route was developed.

Pyrolysis

The pyrolysis synthesis of II-VI semiconductors has been applied to CdS, CdSe, and CdTe.[24,27] The procedure is carried out under an inert atmosphere by rapidly injecting a mixture of dimethylcadmium ($CdMe_2$) and selenium (Se) in trioctylphosphine (TOP) into hot trioctylphosphine oxide (TOPO). The reactant concentration[50] and temperature of the vigorously stirred reaction are controlled to tune the size distribution, yielding particles ranging from 15 to 115 Å.[27] The procedure gives a narrow size distribution of slightly prolate, aliphatic soluble particles that can be further narrowed by "size selective precipitation."[24,27]

In size selective precipitation the crystallite suspension is slowly disturbed by the addition of a non-solvent, causing the particles to reversibly flocculate, with the largest particles agglomerating and separating first. Size selective precipitation allows the isolation of monodispersed nanocrystals, within the limit of atomic roughness. For the process to work the particles must be of similar shape and the size distribution must be relatively small.[27] It has also been reported that arbitrarily broad distributions can be narrowed.[51]

Katari and researchers developed a version of this pyrolysis procedure that yields spherical single-crystal nanoparticles ranging in size from 18 to 60 Å. In the synthesis, the TOP is replaced with tributylphosphine (TBP), the TOPO is heated to a higher temperature and upon injection of the organometallic mixture, the reaction flask is removed from heat and cooled to room temperature. Larger-sized crystallites are produced by adding the reagent solution to the TOPO in small intervals.[44] High quality nanocrystals can be produced in this manner, although the procedure is plagued with difficulty in controlling the average particle size[27] as changes of 1 °C can heavily influence the average size and size distribution.[44] Furthermore the high temperatures can lead to the decomposition of TOPO, producing "an increasingly complex chemical mixture."[27]

Rutherford backscattering spectroscopy (RBS) studies of particles produced by this method indicate that the nanoparticles are consistently Cd rich, with a Cd:Se ratio of 1.2:1 at small sizes and 1.15:1 at larger sizes. Apparently the superior binding of TOPO to Cd over TOP to Se results in a non-stoichiometric surface layer of Cd.[52] Although there remains research to be done,[53] there is not currently a way to precisely control or tune stoichiometry.

The as-synthesized nanocrystals are capped with TOP/TOPO, protecting the Cd from oxidation.[44] The downside to TOP/TOPO is that the caps decompose before vaporizing, leading to the inclusion of decomposed caps in sintered films.[37] Generally, capping groups can be removed and replaced with other capping groups. The most commonly used alternate cap is pyridine, which allows particles to be handled in methanol, aromatics, and pyridine itself.[24] An important characteristic of pyridine is that it vaporizes before decomposing, allowing organic-free films to be formed.[54]

Although pyridine can be completely removed in vacuum,[44] TOP/TOPO caps are not completely removed in the exchange process.[55] Early literature reports indicate that cap exchange is complete,[54] but recent work has shown that 10%-15% of the original TOP/TOPO caps remain.[55] Various exchange conditions have been reported to yield no appreciable change in capping group coverage. It is suggested that capping groups can bind to several Cd sites, leading to the observed stability.[55]

Due to the persistence of TOP/TOPO capping groups, it became necessary to synthesize particles outside of TOP/TOPO. The pyrolysis reaction had been modified during its development and after its publication,[44,50] but in the development of the procedure, TOP and TOPO were employed because they gave superior results.[27] The high quality particles produced in TOP/TOPO are not expected from reactions in alternate solvents.[56] We briefly examined 4-ethylpyridine as an alternate solvent, but focussed on modifying the metathesis reaction because it seemed more promising.

Metathesis

Metathesis has been used to form nanoparticles of a number of chemical species, such as gallium nitride,[57] molybdenum disulfide,[58] and non-binary copper indium gallium diselenide ($Cu(In,Ga)Se_2$, CIGS).[38] The synthesis of CdTe by this method was reported in 1992,[48] and to our knowledge, CdSe has not been synthesized by this route outside of our lab.

$$CdI_2 + Na_2Se \rightarrow CdSe + 2NaI \qquad \textbf{EQUATION 1}$$

Under an inert atmosphere, methanol (MeOH) solutions of cadmium iodide (CdI_2) and sodium selenide (Na_2Se) are added to MeOH, producing CdSe, and the soluble byproduct, sodium iodide (NaI) (**EQUATION 1**).

The reaction is instantaneous, turning the reaction mixture red and precipitating the nanoparticle product. The particles are isolated by repeatedly settling, decanting, and re-suspending the particles, or by repeatedly filtering and washing the particles. The resulting nanoparticles are MeOH capped. Although CdTe nanoparticles have been reported to re-suspend in MeOH,[37] the CdSe nanoparticles synthesized as a part of this work do not. They suspend in pyridine, though, which is known to act as an effective capping group for CdSe nanoparticles.[24]

The published metathesis procedure is relatively simple and gives the desired product with essentially quantitative yields[48] and a 1:1 stoichiometry as determined by X-ray photoelectron spectroscopy (XPS),[37] but the synthesis is hindered by a broad size distribution.[37,59] As an example, metathesis has been reported to produce a distribution of CdTe sizes ranging from 33 to 85 Å, much broader than the 31 to 47 Å range reported for CdTe nanocrystals synthesized by pyrolysis.[37] Still, metathesis has been successfully used to synthesize CdTe nanoparticles for spray deposition for solar cell fabrication. In such a synthesis the nanoparticles were formed at a reduced temperature and are reported to range from 25 to 75 Å in diameter.[37] When forming CdSe particles by this route, however, transmission electron microscopy (TEM) indicates that the majority of particles are ~38 Å in diameter. While TEM is not as sensitive to identifying smaller particles as some other methods,[59] very few particles were observed with diameters below 30 Å. Such relatively large particle sizes are expected to prevent low temperature, plastic-compatible processing.

While reported to be suitable for the production of CdTe, without modification metathesis does not produce CdSe particles small enough for low temperature processing. It is reported that size is controlled by the temperature of the reaction,[48] and with MeOH freezing at -98 °C, there is little room to drop from the -78 °C of the dry ice bath used to cool the reaction in the existing procedure. Such a small temperature change is expected to have a minimal effect on the smallest size of the particles.[48,59]

Because the majority of CdSe particles produced by metathesis are outside the size regime of interest, we needed to modify the metathesis approach. As in the

pyrolysis reaction, the strategy was to alter the nature of the reaction medium. Instead of finding a weaker solvent as in the case of pyrolysis, a stronger solvent was sought to suppress the particle growth relative to nucleation.

To our knowledge, outside of our lab the metathesis reaction has not been modified for the formation of CdSe. A series of modified metathesis procedures were carried out at room temperature in a glove box and the products compared by their UV-Vis spectra. Pyridine and poly-vinylpyridine (PVP) were introduced into the MeOH reaction medium in an attempt to retard particle growth. Similar reaction conditions have previously been used to form a variety of metal selenides for solar cell fabrication.[38,60] In such reactions, pyridine was not intentionally used to slow particle growth, but was used as a solvent for the metal iodide reagents.[38] Particles produced from these metathesis reactions were amorphous and ranged from 10 to 30 nm in size.[60]

Experimental Methods

Glassware was oven-dried and reagents were of the highest purity available except where noted.

A Hewlett Packard (HP) 8452 Ultraviolet-Visible (UV-Vis) spectrophotometer was used for gathering UV-Vis spectra and a Jeol Jem-2010 Electron Microscope was used for TEM and energy dispersive x-ray spectroscopy (EDX). Samples for TEM were prepared in a glove box by depositing pyridine-based CdSe colloids onto amorphous carbon coated Cu grids (Ladd).

Samples for XPS were prepared on an *n*-doped doped (Phosphorous (P) doped) Si wafer by repeatedly depositing CdSe particles synthesized by both metathesis and pyrolysis. The metathesis samples were heated at 350 °C and the pyrolysis samples heated at 400°C, both for 30 minutes. A Physical Electronics 5200 C X-ray Photoelectron Spectrometer with a Mg K_α non-monochromatized source at 300 W was used.

Rutherford backscattering spectroscopy (RBS) was performed at Vanderbilt University.

The pyrolysis method used was a modified procedure[50] based on the methods outlined by Murray and coworkers in 1993. Reactions were carried out in a closed system under nitrogen in a fume hood. The reagents were prepared in a glove box, starting with the filtration of $CdMe_2$ (Organometallics) through a 0.2 μm Teflon filter (Millipore). A 1 *M* standard solution of Se in TOP was prepared by dissolving Se shot (Alfa Aesar) in TOP (Fluka) overnight. The filtered $CdMe_2$ and TOP-Se solution served as the stock for a number of reactions.

Outside of the glove box, the reaction apparatus was set up. TOPO (30 g, Alfa Aesar) was weighed into a 250 mL round bottom flask, a stir bar added, and the flask fitted with a Vigreaux column and nitrogen/vacuum inlet, a thermometer, and a wire-tied rubber septa. The flask was placed under vacuum and heated at 120 °C for 2 hours. The flask was then opened to nitrogen and the temperature increased to approximately 300 °C.

Inside the glove box, 16 mL of TOP were taken into a 20 mL polypropylene syringe (Aldrich) and half dispensed into a scintillation vial. A 250 μL syringe was then used to transfer 200 μL of $CdMe_2$ to the TOP, and the remaining TOP added to the vial. Finally 4 mL of the 1 *M* TOP-Se stock solution were added to the vial and the entire mixture loaded into the syringe. The syringe was outfitted with a disposable needle (BD) and removed from the glove box.

The syringe was then used to rapidly inject its contents into the hot, vigorously stirred TOPO, causing a heavy reduction in the reaction temperature. The reaction was immediately removed from heat and after cooling to ~70 °C 10 mL of butanol (Aldrich) were added to prevent the reaction mixture from solidifying.

After cooling to room temperature, the reaction mixture was transferred to an Erlenmyer flask and the particles were isolated by metering MeOH into the reaction until the broth became cloudy. At this point an additional 2 mL of MeOH were added and the mixture was centrifuged. The supernatant was kept and an excess of MeOH added to force the majority of the remaining particles out of solution. After centrifuging, the particles were collected in butanol and the size distribution further narrowed, or the particles were taken up in pyridine for cap exchange. The supernatant was allowed to sit under N_2, and the particles that precipitated onto the flask's walls were collected as a separate sample.

Cap exchange was carried out by suspending the precipitated particles in pyridine. After stirring at 60 °C for a minimum of 6 hours, the nanoparticles were precipitated out by adding hexane. The particles were collected after centrifugation and were re-suspended in pyridine and the process repeated at least twice more.

In modifying the pyrolysis reaction, 4-ethylpyridine was used as a solvent for the reaction. Because Se is not soluble in 4-ethylpyridine or trioctylamine, TOP was used as the solvent for Se. Reaction procedures for the 4-ethylpyridine reaction followed those for TOP/TOPO, but with injection at 170 °C. Butanol was not added to the reaction upon cooling, but MeOH was added in an attempt to force the particles to flocculate.

Metathesis reactions were based off of a procedure published by Kaner and coworkers in 1992.[48] The nanoparticle preparation was performed under a nitrogen atmosphere in either a glove bag or a glove box. CdI_2 (7.4×10^{-4} mol, Alfa Aesar) was dissolved in 50 mL MeOH (0.015 *M*, Aldrich) and cooled in a dry ice/acetone bath. Na_2Se (7.4×10^{-4} mol, Alfa Aesar) was similarly dissolved in 50 mL MeOH (0.015 *M*) and cooled. The reagents were then poured into a beaker with 30 mL chilled MeOH, reacting instantaneously to yield a red solution. The particles precipitated from the solution and were collected by centrifuging the mixture and then decanting, or by filtering the mixture. In both cases the isolated particles were repeatedly washed with MeOH to remove the soluble byproduct, NaI. Isolated particles were then taken up in pyridine (Aldrich).

A series of modified metathesis reactions were carried out in a glove box at room temperature. Standard 0.015 *M* solutions of CdI_2 and Na_2Se in MeOH were made and equimolar amounts of these stock solutions (5 mL) were rapidly combined in a disposable centrifuge tube (Corning) containing a reaction solvent (5 mL). The reaction medium consisted of a mixture of MeOH and pyridine or PVP (2% cross-linked, Aldrich). Additional experiments introduced ~20% pyridine into the stock solutions to determine if the premixing of pyridine in the reagents' solvent would alter the course of the reaction. In another experiment pyridine was added to the stock solutions to dilute them by a factor of 2 to monitor the effect of changing the concentration of the reactants. Lastly, a reaction was carried out at an elevated temperature (near 100 °C) to monitor the influence of heating on particle growth.

Results and Discussion

In comparison to published UV-Vis spectra, the nanoparticles synthesized by pyrolysis have a small size distribution with the majority of the particles 20 Å in diameter or less (FIGURE 1). TEM shows that the particles are fairly uniform in size and are ~25 Å (FIGURE 2), but it is difficult to determine precisely where the boundaries of the particles are and whether this sample area accurately reflects the size distribution. Some areas appear amorphous, and others appear as particles fused together by the electron beam, indicating that there are particles with crystalline areas too small to observe. Because particles can size selectively precipitate from solution during the preparation of the TEM grid, the observed 25 Å may not accurately reflect the bulk of the size distribution. It should also be noted that researchers have had difficulty resolving particles smaller than 25 Å with TEM,[27] so particles in this size range may very well go unnoticed or appear amorphous.

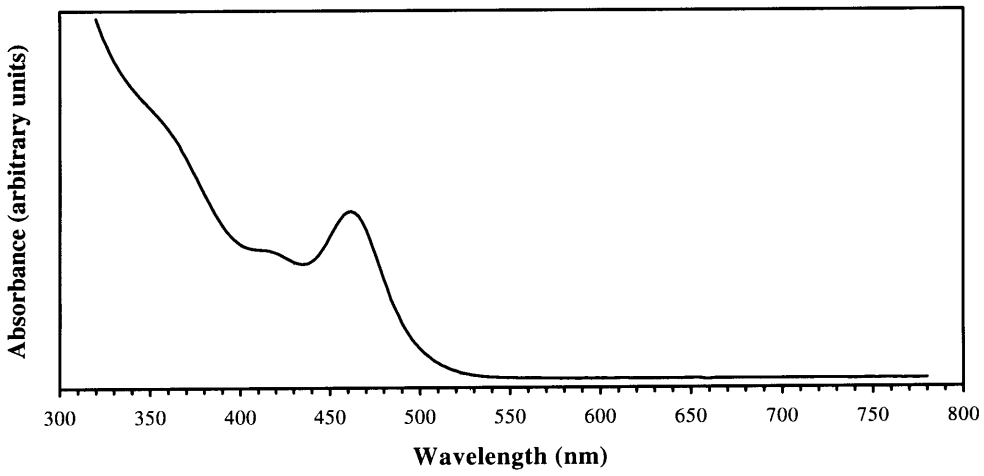

FIGURE 1: UV-Vis spectrum of CdSe nanoparticles synthesized by pyrolysis. Comparing to previously published data,[24,27] the particles average 20 Å in diameter.

For particles synthesized by pyrolysis, UV-Vis spectra demonstrate that the injection temperature effects the average particle size, as an injection at 293 °C was observed to lead to a peak at 470 nm and an injection at 304 °C led to a peak at 484 nm. Injection at 273 °C had a similar effect on the observed absorbence,

dropping it to 460 nm. The difference in average particle size at 460 and 484 nm is approximately 3 Å, about the equivalent of one atomic plane.

XPS of heat-treated films of CdSe particles indicates that pyrolysis forms highly disproportionate particles. The Cd:Se ratio is ~2:1, but more importantly P is present, indicating that the P-based capping ligands are not fully removed in the cap exchange or heat treatment. RBS confirms the presence of P, but is not clean enough to reliably determine the Cd:Se stoichiometry.

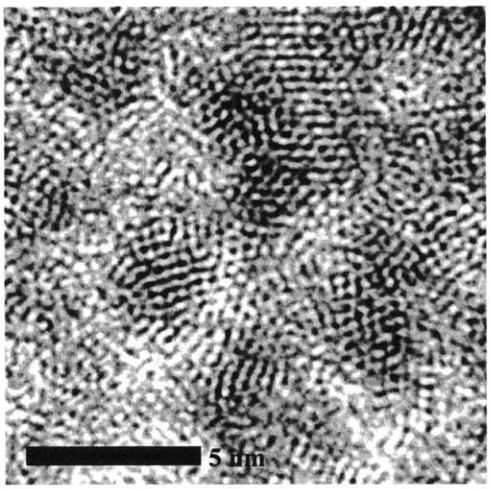

FIGURE 2: TEM image of CdSe nanoparticles formed by pyrolysis. Particles in this region appear to be ~25 Å.

While pyrolysis offers tight control over particle size and distribution, the choice of TOPO as a solvent prevents the isolation of a pure nanocrystalline product. The imbalance in Cd and Se also detracts from the pyrolytic synthesis, although this might be unique to the sample tested, as the ~2:1 Cd:Se ratio observed exceeds even the most disproportionate results previously reported (~1.36).[52] At small particle sizes, any non-stoichiometric surface layer has a large effect on particle stoichiometry, and to further disturb particle stoichiometry Se may be washed off with TOP during cap exchange.[27]

Pyrolytic synthesis in pyridines, amines, and furans is possible,[27] although the tight control over particle size and distribution that make the pyrolysis route attractive is lost in these solvents.[56] For the modified pyrolysis procedure carried out in 4-ethylpyridine, the reaction broth was dirty orange in color and was cloudy with a precipitate. The reaction product did not resemble the TOP/TOPO reactions, or the metathesis reactions. The addition of methanol led to further precipitation, but also led to a separation of liquid layers. This complicated the isolation of any particles, and because the modified metathesis procedure was showing promise, the 4-ethylpyridine synthesis was not investigated any further.

As expected, initial UV-Vis spectra of CdSe particles from the unmodified metathesis reaction are broad and featureless (**FIGURE 3**), indicating that there is a broad distribution of particle sizes.

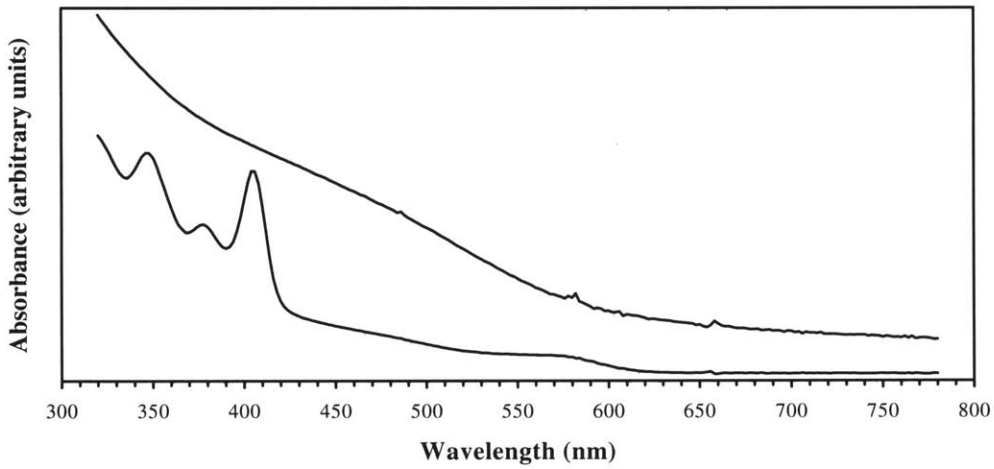

FIGURE 3: UV-Vis spectra demonstrating the size focussing of metathesis-formed CdSe nanoparticles in methanol. The upper spectrum was taken immediately after the reaction and the lower spectrum a day after the reaction. The focussed sample shows bottlenecking near 400 nm and below, and also near 570 nm.

TEM confirms this and shows that most CdSe particles are ~38 Å, although some spherical crystalline areas as small as 20 Å can be seen (**FIGURE 4**).

The dominant large particles are most likely too large to have a melting point amenable to processing with a plastic substrate. EDX indicates that there is a 1:1 Cd:Se ratio for these particles, and does not find Na or I impurities. Similarly, RBS finds a precise 1:1 stoichiometry and no Na or I impurities.

While the unmodified metathesis procedure yields a broad range of sizes, combining the reagent solutions in pyridine instead of methanol produces a tight distribution of very small particles. The influence of pyridine is immediately seen in the reaction, as instead of yielding a deep red solution, the product solution is yellow.

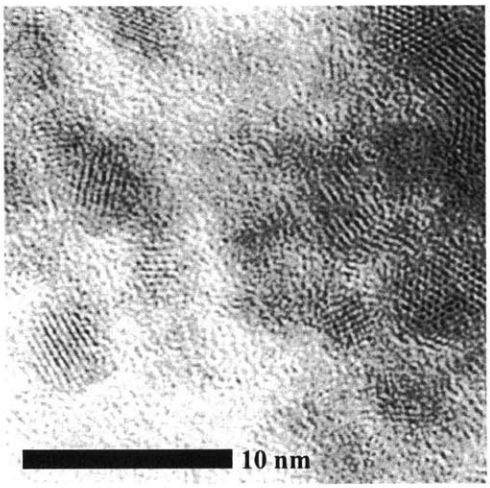

FIGURE 4: TEM image of CdSe nanoparticles formed by metathesis in methanol. UV-Vis spectra correlate well with TEM, indicating that the dominant observable size is nearly 40 Å.

Although the reaction still proceeds in less than a second, pyridine acts to hinder particle growth, yielding smaller particles and a tight size distribution. UV-Vis spectra reveal that as the concentration of pyridine increases the average particle size decreases (**FIGURE 5**).

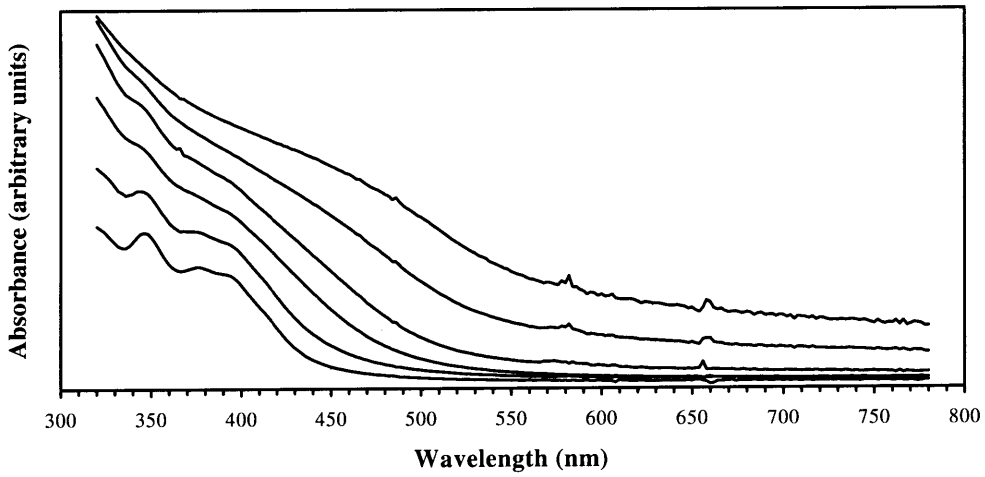

FIGURE 5: UV-Vis spectra series demonstrating the influence of pyridine on the formation of CdSe nanoparticles by metathesis. Increasing the pyridine concentration retards particle growth and reduces the size distribution. The uppermost spectrum represents a sample without any pyridine, and pyridine concentration increases for each subsequent spectrum: 1%, 3%, 7%, 17%, and a maximum of 33% by volume for the lowest UV-Vis spectrum.

At higher concentrations of pyridine the optical spectra begin to show distinct features, indicating that a narrow distribution of particle sizes is formed. The UV-Vis spectra shift and tighten over the course of 24 hours, turning from a strong yellow solution into a pale yellow solution, with absorption features sharpening and settling at slightly higher wavelengths (**FIGURE 6**). The optical features match those previously reported for 17 Å CdSe nanoparticles.[27] We are not aware of any published UV-Vis data for particles smaller than 17 Å.

The shift in particle size is consistent with previous reports. Silver nanoparticles "ripen" over the course of a few days,[51] as do CdS[61] and CdTe[48] particles. Such a shift in size proceeds through "Ostwald ripening," in which the dissolution of material from smaller particles leads to the growth of larger particles.[62] Highly monodispersed systems can arise from this growth mechanism as any "bottleneck" in the growth series will be accentuated. Bottlenecks result from the

stability of a complete, closed structural shell and have been observed in CdSe.[24] At small sizes there are fewer available particle geometries and the relatively high surface energies increase the likelihood of observing a bottleneck in the size series. A number of samples formed by different metathesis methods display the same characteristic absorption features after sitting for 24 hours. Even particles synthesized in methanol, which initially have a very broad and featureless absorption, develop the same characteristic features of the nanoparticles formed in pyridine and show some additional bottlenecking near 570 nm (FIGURE 3).

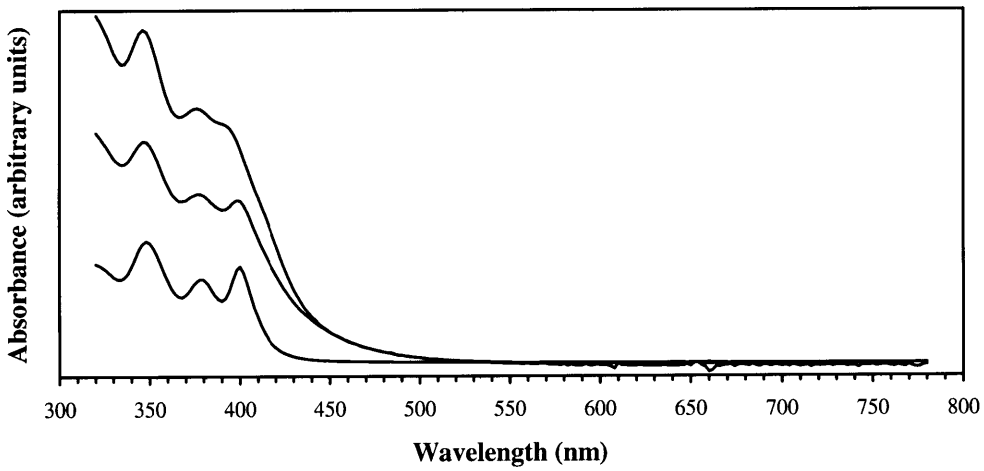

FIGURE 6: UV-Vis spectra series demonstrating the size focussing of metathesis-formed CdSe nanoparticles in pyridine. The uppermost spectrum was taken immediately after the reaction, the middle spectrum a few hours after the reaction, and the lowest spectrum a day after the reaction.

TEM does not resolve the nanoparticles formed in pyridine, but indicates that the particles are small enough to fuse under the electron beam. EDX indicates that the Cd:Se ratio is 1:1 and XPS of heated samples also indicates that there is an approximately stoichiometric Cd:Se ratio. RBS finds a 1.16:1 Cd:Se ratio, indicating that there is a non-stoichiometric surface layer of Cd. Most importantly, XPS performed on heated samples indicates that there is iodine present. One explanation for the observed I impurity is that it might remain bound to the surface of the nanoparticle if there is an excess of the CdI_2 reagent in the reaction medium. EDX and RBS do not find any I or Na in the samples.

It has been suggested that the 17 Å particles are discrete molecular species with a precise stoichiometry.[24] These CdSe species have less than 100 atoms and have a

tetrahedral structure,[56] and thus are often known not as nanoparticles but as nanoclusters. A number of CdSe clusters have been reported,[63] but they are clearly different from the species produced by metathesis. Previous reports indicate that there is a large Se excess in CdSe clusters,[63] while the metathesis-formed particles are either stoichiometric or slightly Cd rich. In Se-rich clusters, organic capping groups bind the four Se corners of the tetrahedron. For a Cd-rich cluster produced by metathesis, I might bind to the Cd corners, accounting for the observation of I by XPS. While the stoichiometry of larger nanoparticles produced by metathesis is consistently 1:1, discrete clusters likely will have a stoichiometric imbalance, which may be what is being observed by RBS.

While the optical features observed for the CdSe nanoclusters match those previously reported for 17 Å nanoparticles,[27] it is more likely that the optical features represent three discrete species.[56] The size distribution around each particle size is very tight, but the monodispersity of the entire sample is compromised by the existence of the three cluster species.

Of the modifications made to the metathesis procedure, the addition of pyridine is the only one to substantially effect the reaction. PVP and reactant concentration have no detectable influence on the reaction. Heating the reaction to ~100 °C results in slightly larger particles and a slightly larger size distribution, but the effect is minimal. The particles are barely larger, and after 24 hours particles formed at room temperature have "ripened" to the slightly larger size of the particles formed at elevated temperatures.

Pyridine's suppression of particle growth was anticipated, but initially there was a concern that adding pyridine to the reaction would hinder the isolation of the product. Pyridine-capped CdSe nanoparticles are soluble in MeOH,[24,27] and it was feared that the product would not precipitate. However, the presence of 2 equivalents of dissolved NaI seems to shift the polarity of the solvent enough to destabilize the particle suspension. This can be observed by adding NaI dissolved in MeOH to a sample of pyridine capped CdSe nanoparticles formed by pyrolysis; the particles agglomerate and precipitate from the MeOH/pyridine solution.

As expected, nanoparticles formed by this modified metathesis route can be isolated as a solid and re-suspended in appropriate solvents. For example, the addition of hexane to a pyridine solution of nanoparticles causes the particles to agglomerate and fall from the solution. The precipitate can then be recovered by

centrifuging, decanting, and re-suspending the solids in pyridine. Such a process leads to no observable change in UV-Vis spectra.

Although pyrolysis is widely regarded as the superior synthetic route to II-VI quantum dots,[29] a modified metathesis approach has proven to be the better route for the intended application domain. The capping group impurities and stoichiometry problems associated with pyrolysis are both major hurdles. While it may be possible to address these issues using a modified pyrolysis procedure, the success of metathesis has prevented the need for further advancing the pyrolytic synthetic route. A simpler procedure with very high yields, metathesis in MeOH is plagued with poor size control and a very large size distribution, leading to large particles that stand little chance of being processed at plastic-compatible temperatures. By moving to pyridine as the reaction solvent, particle growth is inhibited and discrete particle sizes are formed, all below 20 Å. The particles are smaller than those isolated by pyrolysis and are obtained in a near quantitative yield by simply allowing the particles to "ripen" over the course of 24 hours. Although the modified metathesis route does not form tight distributions of particles larger than 17 Å, it is an ideal reaction for forming the very small CdSe nanoparticles desired as precursors for semiconducting TFT channels.

Deposition and Ordering

Approaches to Deposition and Ordering

A number of printing methods can be envisioned for the deposition of a liquid processible semiconductor. In this work we have followed the convention set forth by workers exploring printable organic semiconductors, and have used solution casting as our primary method of deposition. Spin coating is another common deposition technique, but is wasteful[5] and has in some experiments led to poor results relative to casting.[64]

Casting is especially appropriate for this work because it mimics deposition by an ink jet printer, a printing technology being examined in our group for the fabrication of large-featured devices. Our ink jet work has already patterned nanoparticle-based metal inks. The direct stamping or μCP of semiconductors is also an interesting route to pursue, as ultimately any high-quality, fine-featured manufacturing process is likely to draw upon some aspect of soft lithography. To date these printing methods have not been investigated with regards to semiconductor inks.

The continuity of solution cast films is crucial to obtaining reliable device performance. It is also important to determine the thickness of the deposited films, as a thin semiconducting layer is useful for reducing the OFF current of a device.

Additionally, deposition may be important to device performance if the particles can self-assemble to realize long range crystal order. Depending on the nature of the melting or sintering of the particles, particles with pre-aligned atomic planes might yield superior films. If the particle distribution is tightly controlled, the self assembly of deposited nanoparticles into hexagonal close packed arrays is observed.[27,54,65] This occurs when the solvent/cap evaporates slowly enough to allow the nanoparticles to find lattice sites as they fall out of the suspension. Such "superlattices" have been formed with grain sizes as large as 50 μm by carefully evaporating appropriate solvent mixtures.[54] However, the particles' atomic planes do not necessarily line up as a result of this ordering. The alignment of atomic

planes over large areas has been observed in some cases,[50] although it is not clear why this ordering occurs. It has been suggested that highly faceted particles might be more likely to align their crystal lattices.[66] To date this has not been demonstrated.

It is unknown how the ordering of deposited nanoparticles will effect the resultant films, but it is clear that continuity and reproducible film thickness' are vital to fabricating quality devices.

Experimental Methods

All depositions and heat treatments were carried out in a nitrogen-filled glove box.

Pyridine-based solutions of CdSe nanoparticles were deposited by touching the tip of a micro-pipette to the surface of a glass slide or *n*-doped Si wafer. These samples were analyzed with an Olympus BX60 optical microscope, a Digital Instruments Nanoscope IIIa atomic force microscope (AFM), a Jeol JSM-6320 FV Scanning Electron Microscope (SEM), and a Tencor P10 Surface Profiler.

Cu TEM grids with amorphous carbon films were deposited onto with a single drop of pyrolysis-formed 20 Å CdSe nanoparticles in pyridine. The excess solution was wicked away. Similarly, metathesis-formed particles below 20 Å were deposited from pyridine onto Cu TEM grids. The grids were then used as samples for TEM and EDX.

By evaporating the solvent from a known volume of the solution, the concentration of the pyrolysis-formed nanoparticle suspension was determined to be ~10 mg/mL. The metathesis-formed nanoparticle suspension was less concentrated, ~2 mg/mL.

Results and Discussion

Nanoparticles prepared by pyrolysis readily form continuous thin films when cast from pyridine. Optical microscopy shows that a continuous film forms across the width of the drop. After heating the film, AFM and SEM both confirm the continuity of the films. SEM reveals very few defects in the film (**FIGURE 7**), and none are seen with the optical microscope.

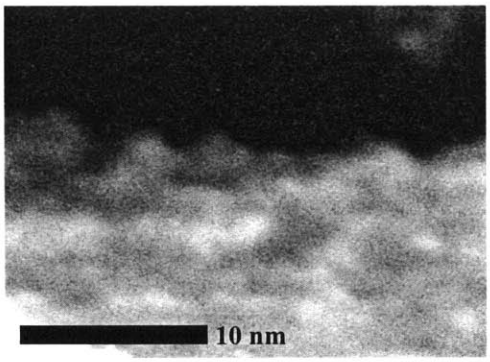

FIGURE 7: SEM image of a fused film of pyrolysis-formed CdSe nanoparticles. The image was taken at the edge of defect to provide contrast to the otherwise featureless, continuous film. There were only a few defects found across the ~10 mm^2 film.

While SEM images indicate that the films are continuous, TEM images show small voids up to 50 nm across. This incomplete coverage most likely relates to the different deposition techniques used in preparing the samples for SEM and TEM, as AFM images also indicate that continuous films are formed by micro-pipette deposition.

Profilometry finds these continuous films to be ~50 nm thick, in the same range as films of organic semiconductors deposited by ink jetting.[67] Larger drops (from a Pasteur pipette, for example) or multiple drops (from a micro-pipette) are observed to cause cracking of the films. The defects are up to several microns wide, but can be readily controlled by the size of the droplet or by the concentration of the solution.

Thin films of metathesis-formed particles also appear continuous. AFM again confirms continuity, and profilometry indicates that the films are ~10 nm thick. AFM finds the films to be smooth, indicating that there are no large agglomerates of particles suspended in solution.

Particles synthesized by both pyrolysis and metathesis form smooth, continuous thin films when cast from pyridine solutions.

The Nature of Melting in Nanoparticles

The melting point depression in metal nanoparticles has been known for some time.[26] In 1991 semiconductor melting point depression was demonstrated in the II-VI semiconductor CdS, "indicating that the phenomenon of reduced melting point in small systems is a general one regardless of the type of material."[28] More recently this behavior has been observed in the semiconductor Si.[9]

Unlike metals, the bonding in semiconductors is "highly directional and covalent."[25] Despite this difference 25 Å gold (Au) and 25 Å CdS nanoparticles both melt at ~300 °C, well below their bulk melting temperatures of 1063 and 1405 °C, respectively.[25,26] The melting point shows a rough inverse dependence on the particle's radius,[9] leading to a sharp drop in melting temperature at particle sizes below 5 nm (**FIGURE 8**). Judging by the melting points of Au and CdS nanoparticles, particles ~25 Å in diameter or less are desirable for keeping processing temperatures plastic-amenable.

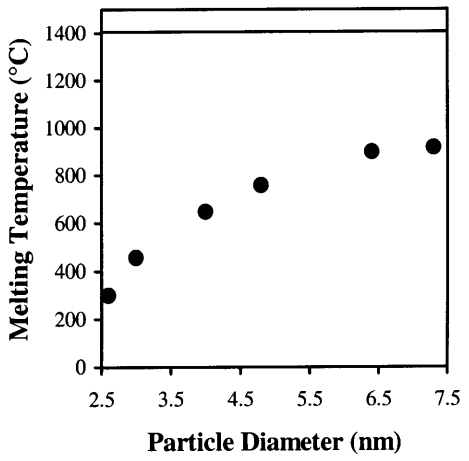

FIGURE 8: The melting point size dependence of the II-VI semiconductor CdS. The data is from the work of Alivisatos and coworkers.[25] The upper line denotes the melting point of the bulk material (1405 °C).

Despite observations that "suggest that melting occurs throughout the particle in a narrow range of temperature,"[9] nanoparticles that are in intimate contact with each other are observed to sinter before melting.[28] This is problematic because fine-grained polycrystalline films are formed with domain sizes "comparable to the size of the nanocrystal initially deposited."[28] This occurs because particles

melt at the surface first, forming a "liquid skin" [68] which fuses the particle with its neighbor. Thus the particle never melts to its core because its effective melting point climbs up the steep melting curve (FIGURE 8) as two particles fuse together. Studies show that nanoparticles will fuse at approximately 2/3 of their reduced melting temperature.[9]

Molecular dynamics calculations for Au clusters show that for larger particles, "liquid patches" first develop at the surface and then propagate to the center of the particle, melting it abruptly. However, particles with fewer than ~250 atoms display no pre-melting effects and the entire particle melts at once.[68] The absence of pre-melting effects at small sizes is important because it suggests that complete melting and subsequent grain growth is possible. Even with surface melting, a rapid thermal or laser treatment could melt the particle throughout, allowing grain growth beyond the dimensions of the nanoparticle.

Polycrystalline Films from Nanoparticle Precursors

A few researchers have used nanoparticle precursors to form semiconductor polycrystalline films. The II-VI semiconductors CdS[32,61] and CdTe[37] have been the most commonly used materials for these studies, mainly because of their use in solar cells. Additionally, CIGS colloids have been prepared and deposited as a part of solar cell fabrication.[38,60] Semiconductor clusters less than 1 nm and as large as 30 nm have been deposited in these studies, requiring fusion temperatures as low as 225 °C and as high as 550 °C.

Sub-nanometer CdS fragments have been deposited and thermally converted to the bulk semiconductor.[32,69] The CdS cluster is bound with an amine and thiophenol, has a precisely known chemical formula, $(N(CH_3)_4)_4Cd_{10}S_4(SC_6H_5)_{16}$, and as such is more appropriately characterized as a molecule than as a nanoparticle. When this semiconductor cluster is deposited from pyridine, there are two distinct stages in the transition from molecular solid to bulk semiconductor. The first transformation occurs at 250 °C, and leaves an intermediate species, $Cd_{10}S_4(SC_6H_5)_{12}$. At 500 °C this cluster loses the remaining phenyl groups as diphenyl sulfide, and leaves behind a stoichiometric CdS film.[32] Despite the very small size of the cluster, relatively high temperatures are required to form the bulk semiconductor film. This is because the heat treatment

does not serve to melt the particle, but instead breaks a formal chemical bond between the cluster and the thiophenol ligand. Such strong inorganic-organic binding interactions are not expected from CdSe-pyridine, as pyridine only weakly caps CdSe particles and has been demonstrated to completely leave the nanoparticle surface under appropriate conditions.[44]

Thiolate-capped CdS nanoparticles ~23 Å in diameter have been reported to fuse at temperatures as low as 200 °C.[62] Formed from the reaction of cadmium acetate with 1-thioglycerol,[62] capping group interactions encourage the particles to form chains when deposited.[61] Fusing these particle chains forms "quantum wires," with parallel wires having a 29 Å spacing.[62] Electrical studies of fused CdS films have been limited,[62] but heat treatments of thioglycerol-capped particles synthesized by a similar route leave "traces" of decomposed organic material.[70] The thiolate ligands have been reported to leave between 200 and 300 °C.[62,70] Lower temperature treatments at 200 and 250 °C do not lead to the recovery of bulk optical properties, indicating there is only a partial fusion of the CdS nanoparticles at these lower temperatures.[62]

Nanoparticle-derived CdTe films have successfully been used in the fabrication of solar cells.[38] By spray depositing CdTe colloids onto a hot substrate, films with large grains can be obtained. Nanoparticles 25 to 75 Å in diameter have been found to form grains 60 to 300 Å across at 400 °C, and grain growth is observed at temperatures as low as 240 °C.[37] There is no residual nanocrystalline topography in these films. Most importantly these films have used in the fabrication of high-quality CdTe solar cells, with the best reported cells having a 2,793 cm^2 active area efficiency of 10.5%.[38]

A similar spray-deposition approach has been used to form pure CIGS films, again for solar cell fabrication. The 10 to 30 nm amorphous nanoparticles were deposited at 550 °C and formed porous films. Grain growth was observed, but researchers did not comment on the size of the grains. The best film exhibited a conversion efficiency of 4.6%.

Experimental Methods

In a nitrogen-filled glove box Cu TEM grids with amorphous carbon films on them were deposited onto with a single drop of pyrolysis-formed 20 Å CdSe nanoparticles in pyridine. The excess solution was wicked away. The grids were then heated at 120 °C under vacuum for 20 minutes to remove the pyridine from the particles, and then placed onto a 400 °C hotplate for 30 minutes. A metathesis-formed pyridine-based suspension of CdSe species smaller than 20 Å was similarly deposited onto grids but was heated for 30 minutes in one step at 350 °C. Grids were used as samples for TEM and EDX, using a Jeol Jem-2010 Electron Microscope.

Samples for XPS were prepared on an *n*-doped Si wafer by repeatedly depositing CdSe particles synthesized by both metathesis and pyrolysis. The metathesis samples were heated at 350 °C and the pyrolysis samples heated at 400°C, both for 30 minutes. A Physical Electronics 5200 C X-ray Photoelectron Spectrometer with a Mg K_α non-monochromatized source at 300 W was used.

RBS was performed at Vanderbilt University.

Samples were prepared for Fourier transform infrared spectroscopy (FTIR) by solution depositing the material, letting it dry, and then annealing it at 400 °C. The product was scraped from the substrate and analyzed on a Nicolet Magna IR 860.

Results and Discussion

Nanoparticles formed by both metathesis and pyrolysis fuse when heated. The domain size, stoichiometry, and morphology of fused films differ according to the synthesis used to form the nanoparticles.

At lower magnifications, TEM indicates that fused 20 Å particles synthesized by pyrolysis form small oblate crystalline domains. They are up to 8 nm long, with an aspect ratio of ~2:1. Many domains still appear spherical, though. High magnification shows that some of the larger crystalline domains have the overall

shape of two or three nanoparticles, indicating that these particles came together to form a single crystalline grain (**FIGURE 9**). Generally, crystal domains appear to result from the fusion of two particles, are ~5 nm across, and a nanocrystal-like morphology is seen.

EDX executed with SEM and TEM instruments gives different ratios of Cd:Se for particles synthesized by pyrolysis. The SEM EDX indicates that there is a large excess of Se (~2:1 Se:Cd) while the TEM EDX indicates that there is a large excess of Cd (~2:1 Cd:Se). The Si substrate used for the SEM samples probably inflates the Se peak because a Si peak sits close to it. However, there is not an analogous situation in the TEM EDX to explain the disproportionate ~2:1 Cd:Se stoichiometry. In fact, XPS confirms the Cd:Se ratio to be ~2:1 Cd:Se. This could result from a non-stoichiometric surface layer of Cd on the particles and/or from stripping TOP-Se groups during cap exchange. It is unlikely that disproportionation occurred during annealing, as this is not observed when annealing bulk CdSe.[71]

Of greater concern is the detection of P by both EDX and XPS. While the XPS samples are deposited onto a P-doped Si wafer, the observed P:Si ratios are ~1:1, much higher than what would be expected from a dopant. For the samples prepared for TEM, there is not a source of P other than the TOP and TOPO used in the synthesis of the nanoparticles. FTIR also indicates that the TOP/TOPO capping groups or their decomposition products remain behind in the polycrystalline films.

The observation of P in films of nanoparticles confirms that the TOP/TOPO caps have not been entirely exchanged and do not leave the nanocrystal surface during heating.

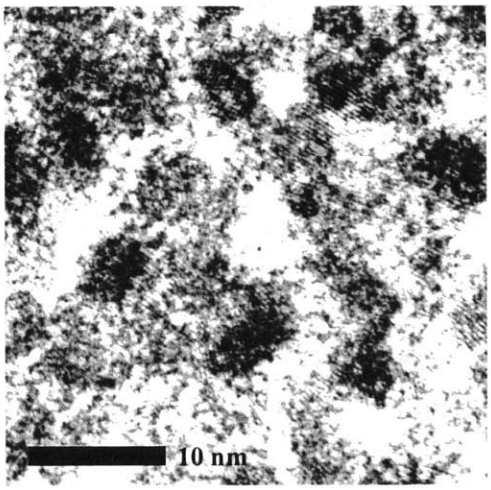

FIGURE 9: TEM image of fused CdSe nanoparticles formed by pyrolysis. A number of the grains appear to result from the fusion of two nanoparticles.

The inability to remove ~10%-15% of surface TOP/TOPO groups from nanoparticles has been reported,[55] but when our investigations began we were not aware of this work. Previous reports had stated that "entirely inorganic arrays"[54] with a "clean nanocrystal surface"[44] could be deposited from pyridine. The presence of TOP/TOPO is a severe problem as even 10% of the original surface coverage is a large amount of impurity; approximately 30% of the particle consists of atoms at the surface and each capping group contains 24 C atoms. Early work on the spray deposition of CdTe used TOP/TOPO capping groups. It was found that the capping groups decompose before vaporizing, leaving large amounts of C impurities in the sintered films.[39]

TEM images of fused particles formed by metathesis indicate that a number of particles fuse together to form larger grains. Generally, the crystalline areas are larger than those observed for pyrolysis-formed particle-derived films. Grains up to 15 nm across are seen and few regions have nanocrystalline morphology (**FIGURE 10**). These grain sizes approach the 20 to 40 nm observed in CdSe TFTs.[72]

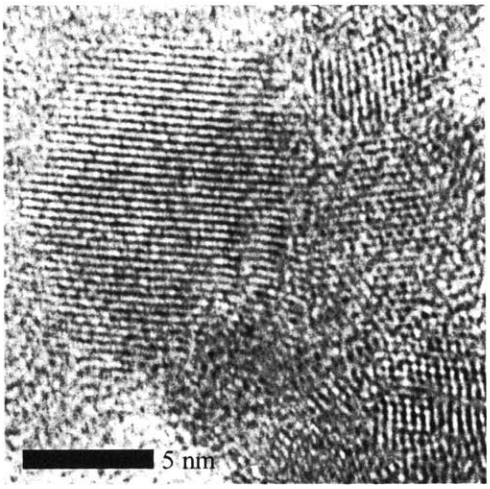

FIGURE 10: TEM image showing long range crystal order resulting from fusing CdSe nanoparticles formed by metathesis in pyridine at 350 °C. Grain sizes are slightly less than those reported for CdSe TFTs.[72]

XPS indicates that the Cd:Se stoichiometry is much closer to 1:1 than for the pyrolysis-derived films. The observed ratio is 47:53, Cd:Se, with a critical observation being the detection of iodine in the films. When comparing the pyrolysis-derived and metathesis-derived films' XPS data, it is clear that the metathesis-derived films lack P and most of the C found in the pyrolysis-derived films, but that the metathesis-formed particles have introduced another impurity. The iodine content is substantial, with a Cd:Se:I ratio of 43:48:9. XPS is a surface technique, and so the ratio might not reflect the composition of the bulk film. Still, the I impurity is substantial, and should effect the device performance of these films. EDX data disagrees with XPS data, as EDX does not detect I and the Cd:Se ratio of fused nanoparticles is found to be ~3:2.

Heating CdSe nanoparticles leads to the formation of small-grained polycrystalline films. Of the two types of films, films from fused pyrolytic nanoparticles have smaller grains and retain a nanoparticle-like morphology. In contrast, metathetic nanoparticles fuse to form films with grain sizes approaching those found in vapor deposited CdSe TFTs.[72] It is unclear if this grain size results from the initial melting and recrystallization of the small clusters or from the anneal. Because pyrolytic particles do not form these larger grains, either their larger size prevent melting and recrystallization or C-based impurities prevent grain growth during the anneal.

Although the grain size and morphological differences are pronounced, the critical difference in films prepared from metathesis or pyrolysis-formed particles is their chemical composition. Films of fused metathesis-formed particles have stoichiometries close to 1:1, while films of fused pyrolysis-formed particles are disproportionate with Cd:Se ratios of ~2:1. I is seen as an impurity in metathesis-derived films, but is not expected to be as severe a problem as the C in pyrolysis-derived films. The observed P indicates that there is residual TOP/TOPO or decomposition products, which have been shown to contaminate sintered films up to 54 atomic percent.[39]

Thin Film Transistors

History

CdS, CdSe, and Te were used in a number of pioneering TFT efforts in the 1960s and 70s. At this time these materials were used to fabricate the first flexible transistors, deposited onto Mylar, aluminum foil, and even paper, and were used to form a 6×6" active matrix for display addressing in an era when silicon wafers were only 1.5" in size.[42] By 1979, CdSe devices were demonstrated that had been running constantly for a decade.[17] Modern CdSe devices have shown mobilities of 450 $cm^2V^{-1}s^{-1}$, ON/OFF ratios of 10^{11}, and the ability to switch 500 V.[17]

Despite excellent device performance and some simple aspects of processing, CdSe has not been a popular production material for TFTs. CdSe devices can have hysteresis problems and require complex photolithography.[73] Perhaps the greatest problem is the lack of a high mobility complementary logic.[73] CdSe TFTs are *n*-type, and to complement them *p*-type copper-doped germanium TFTs (Ge:Cu) have been fabricated, but with lower mobilities (~10 $cm^2V^{-1}s^{-1}$) and poor ON/OFF ratios.[74,75]

Traditional Processing

In fabricating TFTs, CdSe films are usually deposited by evaporation[76] or sputtering.[77] A common criticism of CdSe is that its stoichiometry is not guaranteed.[76] However, the vapor pressure-temperature curves for Cd and Se_2 are very similar[76,78] and the material is very hard to disproportionate.[76] There is a slight excess of Cd present in evaporated films, but the missing Se atoms serve to increase the *n*-type character of the film.[78]

Protecting the semiconductor-insulator boundary is critical to device performance. This is done by sputter cleaning the insulator prior to semiconductor deposition or

by depositing the insulator and semiconductor in the same pump-down cycle. In fact, entire CdSe devices have been fabricated during a single vacuum cycle.[76]

One of the attractive features of CdSe is that it requires only a low temperature anneal.[72] The anneal is critical to device performance, though, as without it devices show only a small field effect and have very high OFF currents. Annealing is usually done for 1 to 4 hours at 350 °C[72,76,79] in a dry air or nitrogen ambient.[71] At such a temperature CdSe grains will grow until they are near the same size as the film thickness. Higher temperatures (400 °C) and longer anneal times (10 hours) can lead to growth of grains larger than the thickness of the film.[80]

It is not through grain growth that annealing improves device performance. As-deposited films with grain sizes comparable to their thickness do not function well in devices.[72] After the heat treatment the devices perform well, though, as the heat treatment reduces the number of donors and anneals out defects.[72] Se vacancies in the as-deposited film lead to the high donor levels, and so the heat treatment encourages the diffusion of excess Cd to grain boundaries, lowering the number of Se voids.[81]

Indium (In) and indium selenide (In_2Se_3) are often used as dopants[76] and have been demonstrated to assist in grain growth during the anneal.[80] For In-doped CdSe, grain growth does not stop when the grain size equals the film thickness. In fact, for similar anneal times, grains in In-doped CdSe films have been observed to grow to twice the size of their undoped counterparts. Even annealing at 200 °C has been observed to grow grains ~50% larger than the thickness of the film.[80]

Cr,[79] Al,[82] and Au[72] have all been used as contact materials for CdSe. Because the metals diffuse into CdSe during the anneal,[79,82,72] an n^+ region is formed near the electrodes and an ohmic contact is created between the metal and semiconductor.[72] Al and Cr have been shown to laterally diffuse into CdSe at room temperature,[82] and Cr has been observed to penetrate up to 20 μm into a TFT channel during a 4 hour anneal at 400 °C.[79] At such temperatures Cr also improves grain growth, producing up to micron-sized grains near contacts. Below 400 °C, though, grain size is found to be uniform across the channel.[79]

Beyond grain growth and forming an ohmic contact, Cr diffusion can have an effect on device performance in two important ways. Channel lengths can be effectively shortened by Cr diffusion, and more importantly, the extent of Cr

diffusion can control the extent of doping and whether a device operates in enhancement mode or depletion mode. Al does not diffuse as readily as Cr, but studies have not yet addressed if Al diffusion and doping can have the large impact on device performance observed for Cr.[79]

Printed Device Fabrication

Again following the convention set forth by researchers in the area of printable organic semiconductors, the printable semiconductor is solution cast onto a semiconductor-less TFT structure fabricated by traditional VLSI processes (**FIGURE 11**). After evaporating the solvent the device is heated, cooled and then encapsulated with a polymer to protect the semiconductor.

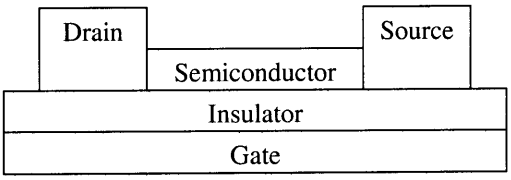

FIGURE 11: Device structure of a bottom gate TFT. The semiconductor is a thin film of CdSe, fused from solution cast nanoparticles.

Experimental Methods

Test wafers were prepared in a clean room at the Microsystems Technology Laboratory (MTL) at MIT. Bottom-gate transistor structures were fabricated without any semiconductor in the channel. The channel length was either 3 or 8 μm and the channel width was 240 μm. The electrodes were connected to a large pad for ease of contact and consisted of 100 nm Cr with an overcoat of Au. The oxide was 80 nm thick thermally grown SiO_2, and the heavily doped Si gate was common to all of the devices. Each 100 mm wafer had ~64 devices.

The nanoparticles formed by pyrolysis that were deposited had an average size of 20 Å. The nanoparticles formed by metathesis that were deposited were tetrahedral-shaped discrete size species smaller than 20 Å.

In a glove box, CdSe nanoparticles were deposited onto the wafer by touching a micro-pipette to the surface over the channel region of the wafer. After the solvent

evaporated, more semiconductor was deposited or the wafer was heated on a hot plate. Heat treatments at 150, 250, 300, and 350 °C were carried out. There were two general types of heat treatment, a ramp up and a thermal shock. The ramp up placed a wafer on the hot plate and gradually brought the temperature to the anneal temperature. The thermal shock program put the wafer onto the hot plate that was already at the anneal temperature. For both programs the duration of heating at the peak temperature was generally 30 minutes.

After cooling, Norland Optical Adhesive 73, a UV-curable polymer adhesive, was used to encapsulate the semiconductor area.

All devices were tested with an HP 4156A precision semiconductor parameter analyzer. Devices were probed in the dark because the CdSe films are photoconductive. Devices were not probed in the glove box. A drain-source voltage sweep of -5 to 5 V was usually used with a gate voltage sweep of -10 to 10 V.

Calculations

In the linear region, the threshold voltage (V_T) was determined by plotting the drain-source current (I_{DS}) vs. gate voltage (V_G) at a drain-source voltage (V_{DS}) = 1 V and extrapolating to $I_{DS} = 0$, where $V_G = V_T + 0.5V_{DS}$. In the saturation region, V_T was determined by plotting the square root of I_{DS} vs. V_G for a V_{DS} in saturation and extrapolating to the intercept with V_G, where $V_G = V_T$.

Most devices were not pushed into saturation, and so reported mobilities correspond to the linear region unless otherwise mentioned. Mobility in the linear region was calculated (**EQUATION 2**) for all of the V_{DS} in the linear region for $V_G >$ 0 V. The reported values are the average of these calculations.

$$\mu = \frac{L\, I_{DS}}{WC_{ox}\,(V_G - 0.5V_{DS} - V_T)V_{DS}} \qquad \textbf{EQUATION 2}$$

For determining both linear and saturation region mobilities, C_{ox} is the oxide capacitance, calculated by dividing the permittivity of the oxide by its thickness. L and W refer to the length and width of the semiconductor channel. Saturation

mobility was calculated (EQUATION 3) for all V_{DS} in the saturation region for V_{DS} = 10 V. The reported values are the average of these calculations.

$$\mu = \frac{2L\, I_{DS}}{WC_{ox}\,(V_G - V_T)^2} \qquad \text{EQUATION 3}$$

Sub-threshold slope was determined directly from a plot of $\log(I_{DS})$ vs V_G.

Results and Discussion

As expected, transistors employing nanoparticles formed by pyrolysis generally fail. The devices are inconsistent, and only rarely display any field effect. We attribute the general failure of these devices to the inclusion of decomposed capping group P and C impurities in the sintered films.

In contrast, metathesis-formed particles generally produce well-behaved devices with reproducible characteristics. There are individual devices that fail or deviate from the characteristics of neighboring devices by an order of magnitude, but the majority of devices work and compare favorably with each other. We have yet to assess whether the semiconductor or wafer is the source of non-uniformity in some of the devices.

The heat treatment is found to have a large impact on the amount of current passed by devices (TABLE 3). For low temperatures, no field effect is seen, indicating that the particles are not sintered. In fact, the electrical characteristics of films treated at 150 °C are identical to those of films of unheated particles. The unheated particles are very resistive and do not pass any more current than the ~10 pA that leak through the wafer.

Peak Temperature (°C)	Peak Mobility ($cm^2V^{-1}s^{-1}$)
150	None
250	0.01
300	0.16
350	2.05

TABLE 3: Comparison of the peak charge carrier mobility observed in nanoparticle-derived CdSe polycrystalline thin films for various anneal temperatures.

Somewhere between 150 and 250 °C there is a point at which the particles sinter to form a polycrystalline film, as devices heated at 250 °C and above demonstrate a reproducible field effect (**TABLE 3**).

The heat treatment at 250 °C was a thermal shock treatment in which the wafer was placed on a pre-heated hotplate and annealed for 30 minutes. The best device to come from this process has a mobility of 0.013 $cm^2V^{-1}s^{-1}$ and an ON/OFF ratio of 185 with a -10 to 10 V gate sweep at V_{DS} = -5 V (**FIGURE 12**). Unlike most devices fabricated at higher temperatures, this device's I-V curves were asymmetric.

Devices were heated at 300 °C in both a thermal shock treatment that lasted for 30 minutes and a slow ramp in which the wafer was heated in increments of 20 °C per minute up to 300 °C and annealed for 2 hours. The highest mobility for the temperature-ramped devices is 0.16 $cm^2V^{-1}s^{-1}$ with an ON/OFF ratio of 35 for a -10 to 10 V gate sweep at V_{DS} = -5 V. The highest ON/OFF ratio for that voltage sweep is 450 with a mobility of 0.08 $cm^2V^{-1}s^{-1}$. The average mobility is 0.04 $cm^2V^{-1}s^{-1}$ and the average ON/OFF ratio for a -10 to 10 V gate sweep is 165. The 30 minute thermal shock treatment gave devices with lower ON and OFF currents, giving lower mobilities than the slowly annealed devices, but giving higher ON/OFF ratios. For the same gate sweep and V_{DS}, the average ON/OFF ratio is 7.4×10^3, with the best device having a value of 8.6×10^3. At the same time the ON current and mobilities drop, making the average mobility only 0.008 $cm^2V^{-1}s^{-1}$.

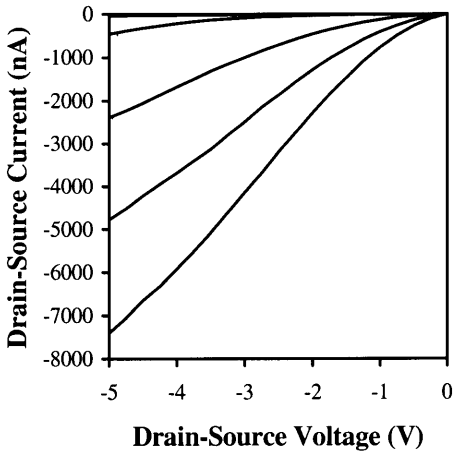

FIGURE 12: Current-voltage characteristics of a device with a semiconducting layer fused at 250 °C. V_G values run from -10 to 10 V in 5 V steps, with 10 V producing ON currents with the greatest magnitude. The ON/OFF ratio is 185 at -5 V V_{DS} and a gate sweep of -10 to 10 V. Mobility in the linear region is 0.013 $cm^2V^{-1}s^{-1}$.

Similar to the devices prepared at 300 °C, devices heated at 350 °C were subjected either to rapid heating by placing the wafer onto a preheated hot plate,

or by gradually ramping up the temperature. Both treatments lasted for 30 minutes, with the thermal shock treatment giving devices with higher ON currents and mobilities, but lower ON/OFF ratios, and the ramped procedure giving devices with lower mobilities but improved ON/OFF ratios. On average, devices gently ramped to 350 °C have a mobility of 0.10 $cm^2V^{-1}s^{-1}$ and an ON/OFF ratio of 400 for a -10 to 10 V gate sweep at V_{DS} = -5 V. Devices submitted to a thermal shock treatment have much higher mobilities, peaking at 2.05 $cm^2V^{-1}s^{-1}$ and averaging 1.21 $cm^2V^{-1}s^{-1}$, but also have much lower ON/OFF ratios for the same gate sweep and V_{DS}, averaging only 21. One outstanding device has an ON/OFF ratio of 1.3×10^3 at V_{DS} = -5 V for a -10 to 10 V gate sweep and has a carrier mobility of 0.26 $cm^2V^{-1}s^{-1}$ (**FIGURE 13**).

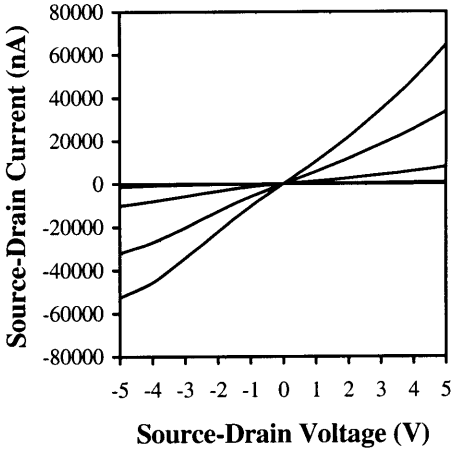

FIGURE 13: Symmetric current-voltage characteristics of a device at varying V_G. V_G values run from -10 to 10 V in 5 V steps, with 10 V producing the ON currents with the greatest magnitude. The ON/OFF ratio is 1270 at -5 V V_{DS} and a gate sweep of -10 to 10 V. Mobility in the linear region is 0.26 $cm^2V^{-1}s^{-1}$. The CdSe was fused at 350 °C.

Some devices saturate for positive V_{DS} (**FIGURE 14**). No saturation is observed at negative V_{DS}. For a given device V_T in the saturation region compares favorably with V_T in the linear region (**FIGURE 15**), and the mobility in the saturation region, 0.058 $cm^2V^{-1}s^{-1}$, compares well with the mobility in the linear region, 0.065 $cm^2V^{-1}s^{-1}$.

The subthreshold slope is determined from a logarithmic plot of I_{DS} vs. V_G for a device in saturation (**FIGURE 16**). The subthreshold voltages range from 4 to 17 V/decade. On average the subthreshold slope is 11 V/decade, with most devices falling between 8 and 13 V/decade.

At 350 °C devices were prepared with different semiconductor thickness'; a single drop of semiconductor suspension was used for some devices, and 5 drops were used for others. While profilometry indicates that a single deposited layer is 10 nm thick, it is unclear if all areas are evenly covered, and so the extra depositions were to ensure that coverage was complete. Comparing the two types of devices, it is clear that the added semiconductor thickness increases the current

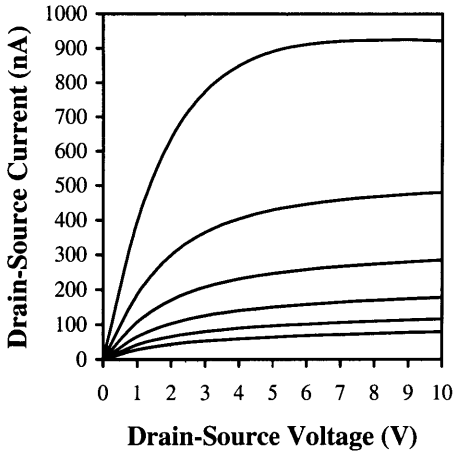

FIGURE 14: Current-voltage characteristics of a device in saturation at varying V_G. V_G values run from 5 to 10 V, with 10 V producing the highest ON currents. Mobility in saturation is 0.058 $cm^2V^{-1}s^{-1}$ and compares well with the linear-region mobility of 0.065 $cm^2V^{-1}s^{-1}$. The semiconductor was fused at 300 °C.

at V_G = 0 V, but that the ON current changes minimally. Subtracting the current at V_G = 0 V from the ON current for the two types of devices indicates that there is no difference in the magnitude of the field effect. There is no additional semiconducting effect gained in going to layers thicker than that resulting from a single deposited drop, demonstrating that a single drop is continuous and that its coverage is complete.

Across all of the devices a trend emerges; increasing the temperature of the heat treatment increases the mobility by increasing the ON current. The OFF current also increases, keeping ON/OFF ratios lower than desired ($>10^5$).[83] The highest ON/OFF ratios observed, found in the devices treated by thermal shock at 300 °C, come paired with some of the lowest mobilities. Meanwhile, the highest mobilities, found in the devices treated by thermal shock at 350 °C, are found in devices with some of the lowest ON/OFF ratios.

There are devices that have both high mobility and high ON/OFF ratios, but generally there is a trade off between mobility and ON/OFF ratio.
Research on organic semiconductors has demonstrated that the ON/OFF ratio is proportional to the mobility divided by the conductivity. It has also been shown that dopants increase both conductivity and mobility, but increase conductivity faster. This means that as doping increases the mobility, it also decreases the ON/OFF ratio.[83] Unlike nanoparticle-derived TFTs, traditional CdSe devices have very low OFF currents.[17] This difference indicates that the nanoparticle-derived channel is doped so that even when turned off, the device can pass considerable current. The CdSe films in question could be doped by Cr diffused from the contacts,[79] by the I impurities found by XPS, or by any non-stoichiometric Cd or Se,[49] leading to improved mobilities and decreased ON/OFF ratios. Why this is exaggerated at high anneal temperatures is undetermined, but high temperatures

should increase Cr diffusion into the channel. If the extent of Cr diffusion is determining the amount of doping, then the channel should not be saturated with Cr. There is no observed change in device performance for 3 or 8 μm channel devices, though. This indicates that the channel is either saturated with the Cr dopant so that the two channel lengths are identically doped, or that Cr diffusion is doping only a very small portion of the channel near the semiconductor/metal interface.

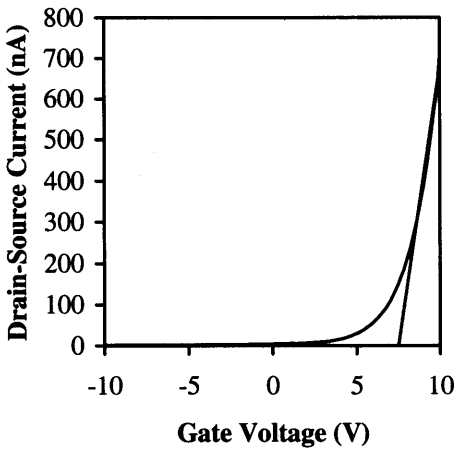

FIGURE 15: A plot of I_{DS} vs. V_G and the linear extrapolation to determine V_T for the device shown in **FIGURE 14**. V_T is 7.5 V.

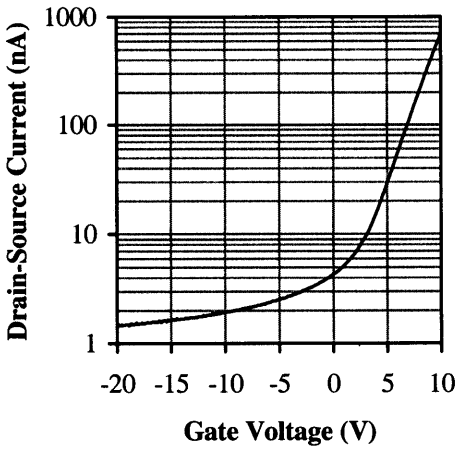

FIGURE 16: Logarithmic plot of I_{DS} vs. V_G to determine sub-threshold slope of the device shown in **FIGURE 14**. The sub-threshold slope is found to be 4 V/decade.

While higher anneal temperatures are generally found to improve mobility, it is unclear how gently or quickly heating the wafer is affecting the film. At 300 °C, gentle temperature increase leads to high mobilities, while at 350 °C thermal shock leads to high mobilities. It is possible that there is a mechanistic difference in the melting or annealing that goes on at 300 and 350 °C, but without carrying out more experiments it is impossible to further speculate on the origins of the observed differences.

Conclusion

The First Printed Inorganic Transistors

CdSe nanoparticles have been solution deposited and thermally processed into thin film transistor channels, demonstrating for the first time that an inorganic semiconductor can be printed. In order to synthesize nanoparticles below 25 Å without tightly bound organic capping groups, a metathesis route initially developed for synthesizing CdTe was modified and applied to the synthesis of CdSe nanoparticles below 20 Å. These nanoparticles form continuous films, free of agglomerates, and upon fusing and annealing form crystalline domains much larger than the nanoparticles.

The highest field effect mobility observed from a solution cast CdSe film is 2.05 $cm^2V^{-1}s^{-1}$. The highest ON/OFF ratio, found in another device, is 8.6×10^3 for a -10 to 10 V gate sweep at V_{DS} = -5 V. For the same voltage sweep a mobility of 0.26 $cm^2V^{-1}s^{-1}$ and an ON/OFF ratio of 1.3×10^3 are found in a single device. These mobilities are believed to be the highest mobilities of any printed semiconductor to date, eclipsing the value of 0.1 $cm^2V^{-1}s^{-1}$ reported for the organic semiconductor P3HT in 1998.[13] In fact, the peak mobilities are higher than the theoretical peak mobilities of organic semiconductors.

The melting point depression of the semiconductor nanoparticles is exploited in the formation of polycrystalline films at plastic-compatible temperatures as low as 250 °C. Higher temperatures are found to form superior semiconducting films, but even films processed at 250 °C have mobilities comparable to printed organic mobilities.[21]

Future Directions

Many research questions remain surrounding the use of nanoparticles as thin film precursors. Advances can be made both in the thermal processing and synthesis of nanoparticles.

While TEM indicates that there is some grain growth beyond the size of the nanoparticles used to form films, it remains to be determined if grain growth occurs through melting and recrystallization or through a slow anneal. Sintering is expected to occur before melting, keeping grain sizes small,[25] but molecular dynamics calculations indicate that very small particles might inherently melt without premelting effects,[68] allowing the particles to access a liquid state and subsequently recrystallize. Although the same issues apply, large grains have been demonstrated in the spray deposition of larger CdTe nanoparticles,[37] in which the nanoparticles come into contact with a heated substrate. Spray deposition, a rapid thermal treatment, a laser treatment, or a μCP deposition, in which the inked stamp comes into contact with a hot substrate, might lead to complete melting and subsequent grain growth regardless of any premelting effects.

Grain growth through melting and recrystallization is very important if an anneal can be avoided. Because the anneal is performed after sintering on the bulk polycrystalline material, there is no melting point depression and the anneal has to be done under traditional conditions. If, however, the anneal can be avoided, the highest process temperature is dictated by the particle's melting point and can be controlled through particle size. As such, in addition to studying the nature of grain growth, a number of temperature studies need to be carried out to determine where the onset of particle fusion lies.

Beyond thermal processing, the quality of the deposited films can be enhanced through improved particle synthesis. Synthetic research should enable the removal of impurities such as iodine, which may be responsible for the low ON/OFF ratios. Synthetic control over particle stoichiometry is also important, as this, too, can heavily influence device performance.[49]

In addition to improving the purity of the synthesized material, introducing dopants such as In is possible by further modifying the metathesis reaction (EQUATION 4).

$$xCdI_2 + yInI_3 + Na_2Se \rightarrow Cd_xIn_ySe + 2NaI \qquad \textbf{EQUATION 4}$$

Because the product stoichiometry is dictated by the ratios of the reagents,[38] fine control over doping levels should be possible.

This research demonstrates for the first time that nanoparticle-based inks combine the processing advantages of organics with the performance advantages of inorganics. The methods outlined herein for the printing of nanoparticle semiconductors can be generalized for other materials, enabling all-printed inorganic circuitry. Such an all-printed device has yet to be demonstrated, but the high printed mobilities already observed for CdSe are encouraging and demand further investigation.

Acknowledgements

I would like to thank Babak Nivi for fabricating the test wafers; Babak Nivi and Marcin Strojwas for helping with testing devices and device calculations; Mike Frongillo for assistance with TEM and SEM; Elisabeth Shaw for assistance with XPS and AFM; Tim McClure for assistance with the FTIR and profilometry; and Jason Taylor at Vanderbilt University for carrying out the RBS.

I would like to thank Brian Hubert and Saul Griffith for helpful comments on this document.

I would also like to thank the readers of this thesis, Professor Dimitri Antoniadis, Professor Moungi Bawendi, and Professor Joseph Jacobson.

Most of all, I'd like to thank my wife, Savalai Vaikakul, for helpful comments, support, organization, and perspective.

I would also like to gratefully acknowledge the fellowship support of Interval Research Corporation and Motorola.

This work made use of MRSEC Shared Facilities supported by the National Science Foundation under Award Number DMR-9400334.

References

[1] B Richmond. Private communication, **1998**.

[2] RS Sposili, JS Im. *Appl Phys Lett*, **1996** (69) *19* 2864.

[3] JS Im, MA Crowder, RS Sposili, JP Leonard, HJ Kim, JH Yoon, VV Gupta, HJ Song, HS Cho. *Phys Stat Sol*, **1998** (166) 603.

[4] N Gershenfeld. *When Things Start to Think*, **1999**, Henry Holt and Company, NewYork, USA.

[5] J Bharathan, Y Yang. *Appl Phys Lett*, **1998** (72) *21* 2660.

[6] Y Xia, GM Whitesides. *Angew Chem Int Ed*, **1998** (37) 550.

[7] DR Lide, ed. *Handbook of Chemistry and Physics 77th Edition*, **1996**, CRC Press, Boca Raton, Florida, USA.

[8] H Uda, H Sonomura, S Ikegami. *Meas Sci Technol*, **1997** (8) 86.

[9] AN Goldstein. *Applied Physics A*, **1996** (62) *1* 33.

[10] J Jacobson. Private communication **1999**.

[11] JA Rogers, Z Bao, VR Raju. *Appl Phys Lett*, **1998** (72) *21* 2716.

[12] RF Service. *Science*, **1997** (278) 383.

[13] H Sirringhaus, N Tessler, RH Friend. *Science*, **1998** (280) 1741.

[14] TN Jackson. Private communication, **1999**.

[15] Y Cao, GM Treacy, P Smith, AJ Heeger. *Appl Phys Lett*, **1992** (60) *22* 2711.

[16] J Tsukamoto. *Advances in Physics*, **1992** (41) *6* 509.

[17] TP Brody. *Information Display*, **1992** (2) 5.

[18] KC Saraswat, V Subramanian, S Jurichich. *Mat Res Soc Symp Proc*, **1997** (472) 439.

[19] HE Katz. Private communication, **1997**.

[20] F Garnier, R Hajlaoui, ME Kassmi. *Appl Phys Lett*, **1998** (73) *12* 1721.

[21] Z Bao, AJ Lovinger, A Dodabalapur. *Appl Phys Lett*, **1996** (69) *20* 3066.

[22] J Jacobson, B Comiskey, C Turner, J Albert, and P Tsao. *IBM Systems Journal*, **1997** (36) *3* 457.

[23] B Comiskey, JD Albert, H Yoshizawa, J Jacobson. *Nature*, **1998** (394) *6690* 253.

[24] CB Murray, DJ Norris, MG Bawendi. *J Am Chem Soc*, **1993** (115) 8706.

[25] AN Goldstein, CM Echer, AP Alivisatos. *Science*, **1992** (256) 1425.

[26] P Buffat, JP Borel. *Physical Review A*, **1976** (13) *6* 2287.

[27] CB Murray. PhD Thesis, **1995**, MIT.

[28] AN Goldstein, VL Colvin, AP Alivisatos. *Mat Res Soc Symp Proc*, **1991** (206) 271.

[29] LE Brus. *J Phys Chem Solids*, **1998** (59) *4* 459.

[30] RW Siegel. *Scientific American*, **1996** (275) *6* 74.

[31] JL Heinrich, CL Curtis, GM Credo, KL Kavanagh, MJ Sailor. *Science*, **1992** (255) 66.
[32] N Herron, JC Calabrese, WE Farneth, Y Wang. *Science*, **1993** (259) 1426.
[33] AP Alivisatos, AN Goldstein. US Patent 5,262,357 **1993**.
[34] AN Goldstein. US Patent 5,559,057 **1996**.
[35] AN Goldstein. US Patent 5,576,248 **1996**.
[36] M Pehnt, DL Schultz, CJ Curtis, DS Ginely. US Patent 5,711,803 **1998**.
[37] DL Schultz, M Pehnt, CJ Curtis, DS Ginley. *Mat Res Soc Symp Proc*, **1996** (426) 349.
[38] DL Schultz, CJ Curtis, RA Flitton, H Wiesner, J Keane, RJ Matson, PA Parilla, R Noufi, DS Ginley. *NREL/SNL Photovoltaics Review*, **1997** 683.
[39] M Pehnt, DL Schultz, CJ Curtis, HR Moutinho, A Swartzlander, DS Ginley. *Mat Res Soc Symp Proc*, **1995** (382) 461.
[40] M Pehnt, DL Schultz, CJ Curtis, KM Jones, DS Ginley. *Appl Phys Lett*, **1995** (67) *15* 2176.
[41] DL Schultz, M Pehnt, CJ Curtis, DS Ginley. *Materials Science Forum*, **1996** (225-227) 169.
[42] TP Brody. *Information Display*, **1997** (10) 28.
[43] AP Alivisatos. *MRS Bulletin*, **1998** (Feb) 18.
[44] JE Bowen Katari, VL Colvin, AP Alivisatos. *J Phys Chem*, **1994** (98) 4109.
[45] JG Brennan, T Siergrist, PJ Carroll, SM Stuczynski, LE Brus, ML Steigerwald. *J Am Chem Soc*, **1989** (111) 4141.
[46] VL Colvin, AN Goldstein, AP Alivisatos. *J Am Chem Soc*, **1992** (114) 5222.
[47] ML Steigerwald, AP Alivisatos, JM Gibson, TD Harris, R Kortan, AJ Muller, AM Thayer, TM Duncan, DC Douglass, LE Brus. *J Am Chem Soc*, **1988** (110) 3046.
[48] RF Jarvis, M Müllenborn, BG Yacobi, NM Haegel, RB Kaner. *Mat Res Soc Symp Proc*, **1992** (272) 229.
[49] U Klement, F Ernst. *Mat Res Soc Symp Proc*, **1997** (472) 131.
[50] C Leatherdale. Private communications, **1998** and **1999**.
[51] JR Heath, CM Knobler, DV Leff. *J Phys Chem* **1997** (101) 189.
[52] J Taylor, T Kippeny, JC Bennett, M Huang, LC Feldman, SJ Rosenthal. *Mat Res Soc Symp Proc*, in press.
[53] J Taylor. Private communication, **1999**.
[54] CB Murray, CR Kagan, MG Bawendi. *Science*, **1995** (270) 1335.
[55] M Kuno, JK Lee, BO Dabbousi, FV Mikulec, MG Bawendi. *J Chem Phys*, **1997** (106) *23* PAGE.
[56] MG Bawendi. Private communication **1999**.

[57] CH Wallace, S Kim, GA Rose, L Rao, JR Heath, M Nicol, RB Kaner. *Appl Phys Lett*, **1998** (72) *5* 596.
[58] JB Wiley, PR Bonneau, RE Treece, RF Jarvis, EG Gillan, L Rao, RB Kaner. *Supramolecular Architecture*, **1992** (26) 369.
[59] M Müllenborn, RF Jarvis, BG Yacobi, RB Kaner, CC Coleman, NM Haegel. *Appl Phys A*, **1993** (56) 317.
[60] DL Schultz, CJ Curtis, RA Flitton, H Wiesner, J Keane, RJ Matson, KM Jones, PA Parilla, R Noufi, DS Ginley. *Journal of Electronic Materials*, **1998** (27) *5* 433.
[61] A Chemseddine, H Jungblut, S Boulmaaz. *J Phys Chem*, **1996** (100) 12546.
[62] A Chemseddine, ML Fearheiley. *Thin Solid Films*, **1994** (247) 3.
[63] S Behrens, D Fenske. *Ber Bunsen Phys Chem*, **1997** (101) *11* 1588.
[64] Z Bao, A Dodabalapur, AJ Lovinger. *Appl Phys Lett*, **1996** (69) *26* 4108.
[65] BO Dabbousi. PhD Thesis, **1997**, MIT.
[66] B Korgel. Private communication, **1998**.
[67] TR Hebner, CC Wu, D Marcy, MH Lu, JC Sturm. *Appl Phys Lett*, **1998** (72) *5* 519.
[68] F Ercolessi, W Andreoni, E Tosatti. *Physical Review Letters*, **1991** (66) *7* 911.
[69] WE Farneth, N Herron, Y Wang. *Chem Mater*, **1992** (4) *4* 916.
[70] T Vossmeyer, L Katsikas, M Giersig, IG Popovic, K Diesner, A Chemseddine, A Eychmuller, H Weller. *J Phys Chem*, **1994** (98) 7665.
[71] JP Szabo, M Cocivera. *J Appl Phys*, **1987** (61) *10* 4820.
[72] A Van Calster, A Vervaet, I De Rycke, J De Baets. *Journal of Crystal Growth*, **1988** (86) 924.
[73] C Reita. *Information Display*, **1993** (2) 10.
[74] J Doutreloigne, H De Smet, J De Baets, I De Rycke, A Van Calster, J Vanfleteren. *Proc Eurodisplay*, **1990** 316.
[75] AM De Cubber, H De Smet, J De Vos, N Carchon, A Van Calster. *IEEE Electron Device Letters*, **1996** (17) *12* 581.
[76] TP Brody. *SPIE*, **1992** (1664) 2.
[77] MJ Lee, Sw Wright, CP Judge, PY Cheung. *International Display Research Conference (IDRC)*, **1991** 211.
[78] E Lueder. *SID*, **1994** 30.
[79] D Waechter, MR Westcott, F Lin, MK Hatalis. *J Electrochem Soc*, **1993** (140) *10* 2994.
[80] MK Hatalis, F Lin, MR Westcott. *Mat Res Soc Symp Proc*, **1990** (164) 87.
[81] A Van Calster, J Vanfleteren, I De Rycke, J De Baets. *J Apply Phys*, **1988** (64) *6* 3282.
[82] GJ Scilla, JJ Wysocki. *J Vac Sci Technol*, **1981** (18) *1* 37.
[83] CD Dimitrakopoulos, AR Brown, A Pomp. *J Appl Phys*, **1996** (80) *4* 2501.